DSP-Based Carrier Acquisition and Tracking for Burst TDMA Mobile Land and Satellite Receivers

By Mohamed K. Nezami
Raytheon Company

The theory of optimum receiver data wireless detection requires synchronization signal parameters that are accurately aligned with those in the transmitter. Therefore, synchronization should be the most robust and reliable element in the receiver design process, ensuring that data detection can continue over deteriorating channels, such as those with fading and large carrier offsets. Furthermore, the available processing time at the receiver for burst-type systems is very short, and computationally efficient techniques are required in order to acquire and track the received signal quickly. Computationally efficient synchronization methods also benefit receiver power consumption.

Carrier frequency offsets can be large due to Doppler shifts or frequency uncertainties in the receiver and transmitter frequency mixing stages [2, 4]. This problem may sometimes be circumvented by imposing stringent requirements on the frequency stability of the transmit and receive oscillators. For example, a receiver with a frequency offset tolerance of 100 hertz, inclusive of Doppler shifts, requires the use of an oscillator with stability better than 0.10 parts per million (PPM). This is a severe constraint given that such an oscillator has to be a temperature-compensated crystal oscillator and (TXCO), which requires large amounts of DC-power and a long warm-up time and is both bulky in size and expensive.

Therefore, we must seek alternate methods for frequency compensation that use less accurate frequency sources. Since the cost-efficient implementation of time division multiple access (TDMA) terminals generally requires extensive use of digital signal processing techniques, it may be more convenient to implement frequency offset estimation and correction algorithms that relieve the stringent requirements on the master frequency oscillator in the receiver [7]. Furthermore, it is desired that such algorithms be limited to the digital signal processing part of the radio. This means that conventional techniques, such as analog voltage control oscillator steering, are not favored.

This article describes modeling, analysis and simulation results of an all-digital carrier synchronization algorithm for burst type TDMA signals subjected to additive white Gaussian noise (AWGN) and severe Doppler frequency shift that is relatively large compared to the data rate of the receiver. The algorithm detailed in the coming sections is well suited for an all digital receiver implemented using either digital signal processing (DSP) or ASIC techniques. Although the detailed algorithm is shown here only for BPSK and QPSK TDMA satellite burst receivers, it could easily be extended for applications in other current wireless systems, such as GSM, IS-136, personal handy-phone system (PHS), multimedia cable or local multipoint distribution (LMDS).

Introduction

In TDMA transmission systems, multiple users share the same channel by using the same bandwidth for discrete intervals of time slots. Only one user can access the channel at any time. Time slots are assigned by a network controller for each user frame. Each user terminal has a unique carrier phase and frequency offset, resulting in unpredictable carrier changes from message to message. Currently, to aid acquisition, each TDMA message or frame has a pre-

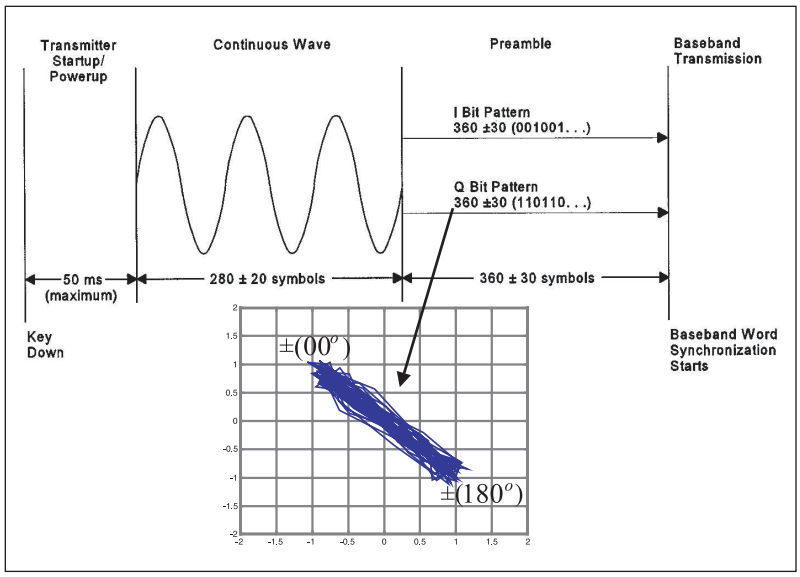

▲ **Figure 1. Typical satellite TDMA preamble.**

amble or training sequence. The preamble is transmitted as the initial part of each communications burst (some systems, such as GSM, have midamble). The preamble typically provides information necessary for signal acquisition and synchronization, including a unique word associated with individual receivers that can be used to resolve carrier phase ambiguity. In some of variable data rate and multitransmission systems (3G), the preamble has a field that indicates the data rate being sent and the modulation type.

The preamble format usually is made up of a continuous wave (CW) followed by a dot pattern (alternating or repeating sequence of ones and zeros), as shown in Figure 1 [1]. Conventionally, the CW portion of the preamble is generated with constant data on both the I and Q signals (real and imaginary part of the received signal are all marks), while the dot pattern portion of the preamble consists of alternating data on the I channel (I = 0 1 0 1 . . .) and an opposite alternating phase symbols on the Q channel (Q = 101010…). The CW sequence (all zeros) creates a CW tone that is commonly used by receivers to recover frequency offsets using some form of feedback loops, such as Costas loops [2]. The 1-0 pattern creates a dot pattern that is also used by the receiver for bit synchronization [2, 3]. Since these overhead bits of the preamble reduce the signaling efficiency, it is desirable that this preamble be as short as possible, yet long enough to allow carrier synchronization with minimal final phase errors.

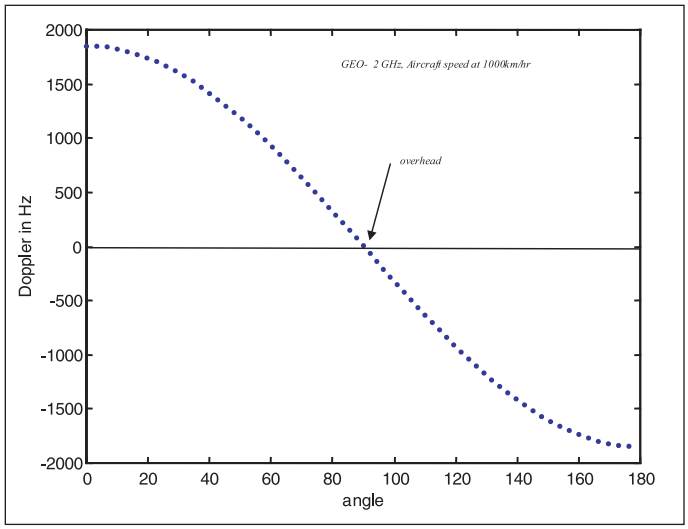

▲ **Figure 2. GEO satellite-to-aircraft Doppler profiles at 2 GHz.**

Causes of carrier frequency offset in wireless receivers

Carrier frequency errors are mostly due to propagation channel effects and transmitter/receiver circuitry of both mobile ground stations (handset) and the satellite transponder (base station). Frequency offsets in mobile communication terminals are due to factors such as oscillator frequency uncertainty, oscillator drift and Doppler effects from vehicular relative motion with respect to the satellite or the base station. Depending on the carrier frequency and the relative velocity between the transmitter and the receiver, such frequency offsets can vary from a few hundred hertz up to several hundred kilohertz. Such large carrier offsets result in increased BER due to reduced receiver sensitivity and phase rotation in the received symbols.

The Doppler frequency shift of the received signal is given by

$$f_d = f_c \frac{v(t)}{c} \cos\big(\alpha(t)\big) \qquad (1)$$

where $v(t)$ is the relative velocity of the receiver terminal with respect to the transmitter in meters/sec, f_c is the carrier frequency in hertz and $\alpha(t)$ is the angle between the relative velocity vector and the signal propagation direction in degrees (satellite or base station elevation angle) [4].

Figure 2 shows the satellite Doppler frequency variations as a function of the angle $\alpha(t)$ for a GEO system operating with f_c = 2 GHz for an aircraft traveling at 1,000 km/hour. The Doppler frequency is minimum (at α = 90 degrees) when the satellite is passing overhead and is maximum (f_d = ±1800 hertz) when the satellite is over the horizon (at α = 0 and 180 degrees). LEO satellites are located at heights of 10,000 to 20,000 km above the equator [4] and have a relative velocity of 1,500 m/s. If the system is operating at 2 GHz, the Doppler shifts (f_d) can be as high as 10 kHz, and the Doppler frequen-

cy shifts can change by up to 250 hertz/seconds. This scenario complicates the carrier frequency offset estimation algorithm, especially when it uses long observation intervals (for typical moderate burst lengths), where it is required that such algorithms account for this continuous change in frequency.

Contrary to LEOs, GEO satellites are located at a height of 36,000 km and do not have any motion relative to a fixed ground terminal. However, due to vehicle velocities of up to 100 km/hour, the ground mobile receivers may experience Doppler shifts of up to 138 hertz for L-band signals. For an aircraft traveling at speeds of 1,000 km/hour, the Doppler frequency shift can be as high as 1800 hertz for 2 GHz systems, as shown in Figure 2.

In addition to Doppler shifts, frequency offsets are introduced due to tolerances of the local oscillator frequencies in the receiver terminal as well as the satellite transponder translator. For example, if the tolerance of the receiver local oscillator is specified at 0.2 PPM for a carrier at 2 GHz, the introduced frequency offset will be 400 hertz. More information on frequency offset system distribution and analysis techniques for multiple access satellite receivers can be found in [5].

Burst TDMA satellite carrier acquisition and tracking

In continuous TDMA satellite modems, such as home satellite receivers or news gathering mobile terminals (ENGS), the user can afford to wait a few seconds for initialization, during which the receiver goes through an acquisition and phase tracking process using conventional slow narrowband analog phase lock loop (PLL) or Costas loop systems.

With burst satellite software based modems, however, the user data burst consumes only a fraction of the overall time frame; hence, long acquisition times contribute an unacceptable level of overhead to the system and substantially reduce the transmission capacity. Thus, burst modems require a special acquisition process that quickly estimate the carrier frequency offsets and phase to perform corrections.

Furthermore, burst systems must adapt to different modulation types. The use of analog PLL or Costas loop is conventionally limited by narrow capture range to twice the loop bandwidth. Contrary to feedback loops, feedforward methods have large capture range and are more suited for rapid acquisition. However, they do tend to have larger tracking variance associated with the received carrier [6, 7].

The literature dealing with the carrier recovery process for preamble or preamble-less based modulated MPSK signals is scarce [2]. The CW-Costas loop can only be used during the CW portion of the preamble, as shown in Figure 1. To extend the operation of feedback carrier recovery loops to acquire and track the received carrier in the presence of modulations during the message portion of the burst, the conventional Costas loop has to be modified and implemented digitally either at baseband or at a bandpass-sampled intermediate frequency (IF). Such loops derive a phase/frequency error signal based on the transition and data decision of both I and Q channels (i.e., real and imaginary parts of the matched filter samples). The decision-aided phase/frequency error is sometimes called a polarity type error detector opposed to the conventional "sine" phase detector used in CW (unmodulated) systems.

Consider the sampled complex signal input into the DSP section of the receiver given by

$$s_r(kT) = I(kT)\cos(2\pi f_r kT + \theta_r) - Q(kT)\cos(2\pi f_r kT + \theta_r) \quad (2)$$

where k is the sample index, T is the sample time and f_r and θ_r are the frequency and phase associated with the received signal. This signal is downconverted to baseband using a digital down converter chip by mixing with a free running complex local oscillator that is usually implemented digitally as a complex numerically controlled oscillator (CNCO) [9] given by

$$y_L(kT) = \cos(2\pi f_L kT + \theta_L) - \cos(2\pi f_L kT + \theta_L) \quad (3)$$

The resultant in-phase and quadrature phase samples produced will be

$$I(k) = 1.\cos(2\pi \Delta f kT + \theta) \quad (4)$$

and

$$Q(k) = 1.\sin(2\pi \Delta f kT + \theta) \quad (5)$$

where $\Delta f = f_L - f_r$ is the carrier frequency offset and $\theta = \theta_L - \theta_r$ is the carrier phase error.

To perform correct data detection, the receiver must estimate and remove Δf and θ from the received signal by compensating the two complex samples in (4) and (5). To do this, the receiver generates an error signal proportional to the magnitude of Δf and θ. Unlike the feedforward algorithms developed in [6, 7], this error signal is not equal to the final offset (immediate estimate); instead, the feedback error signal is used to steer a freely running CNCO [9]. One technique to apply this is to acquire the carrier (frequency offset estimation) during the CW portion of the preamble and perform carrier tracking (phase estimation) during the rest of the burst that extend over the unique world (UW) and the rest of the TDMA frame that contains the transmitted message. The next section develops the mechanism of detecting both the carrier undesired phase and the carrier frequency offsets.

Detecting the carrier frequency offset error signal

During the initial stages of receiver operation, the incoming signal in Equation (2) is received with a large frequency offset; hence, phase tracking or data detection cannot be performed unless the frequency offset Δf is removed. This frequency offset causes power drops in the MF output and a large unprecedented symbol rotation that leads to error in the symbol decision making algorithm.

To acquire and lock the local oscillator (NCO) signal in Equation (3) to the incoming carrier frequency, or produce a baseband that has no frequency translation, an error signal detector, in conjunction with a closed correction loop, senses the amount and direction of this offset and then corrects it. The process of rapid frequency estimation and correction is known as automatic frequency control (AFC).

The loop uses a frequency error detector to bring the initial frequency error Δf rapidly close to zero. However, because it never completely acquires phase offset, another stage of processing is needed to track undesired carrier phase rotations. For this reason, even at steady state, AFC loops alone have a phase error that randomly walks around as AWGN noise perturbs the error detector mechanism. In other words, since the AFC loop is not responsive to phase, the phase reference is not coherant and therefore symbols are not placed at their nominal constellation location, but rather are distributed randomly around it.

For signals that do not contain any PSK modulations (i.e. CW), the frequency error can be generated by correlating the on time received matched filter (MF) sample $z(k)$ and the conjugate of the late MF sample $z^*(k-1)$, as shown in Figure 3. This leads to frequency offset error signal given by

$$Z_k Z_{k-1}^* = \underbrace{[I_k I_{k-1} + Q_k Q_{k-1}]}_{\mathrm{Re}\{Z_k Z_{k-1}^*\}} + j\underbrace{[Q_k I_{k-1} - Q_{k-1} I_k]}_{\mathrm{Im}\{Z_k Z_{k-1}^*\}} \quad (6)$$

The error detector in Equation (6) assumes a CW MF signal; thus, this error signal is valid only during the CW portion of the preamble shown in Figure 1. If the frequency offset recovery is extended over portions of the preamble with data modulations, the error detector can still derive a frequency offset error by passing th emodulated QPSK/BPSK signal thorugh an M-nonlinearity that removes the phase modulations and produces a CW tone, from which an error is extracted. For BPSK, the order of the nonlinearity is $M = 2$, and for QPSK it is $M = 4$. To demonstrate this, assume that the MF QPSK samples with an associated carrier frequency offset Δf are given by

$$c_k = e^{j\frac{\pi}{4}} e^{j(m)\frac{\pi}{2}} e^{j2\pi\Delta f k T}$$

where $m = 0,1,2,3$. By processing c_k using a fourth order nonlinearity, or $[c_k]M = 1.\exp\{j(M2\pi kT\Delta f)\}$, the QPSK phase modulation are removed, resulting in a noisy CW signal containing a fundamental frequency that is equal to M-fold the carrier offset.

Detecting phase error for phase modulated bursts

After carrier frequency offset detection using Equation (6) and correction, the complex MF signal can be represented by an in-phase sample of $I_k = \cos(\theta_k)$ and a quadrature phase sample of $Q_k = \sin(\theta_k)$, where θ_k is the phase error associated with the k^{th} symbol.

If carrier phase tracking is performed during the CW portion of the preamble as in Figure 1, the phase error will be assumed small, or $\theta_k \to 0$, hence $\theta_k \approx \sin(\theta_k)$ and $\cos(\theta_k) = 1$ or $\theta_k = \mathrm{Im}\{z(k)\}$. However, these results will not hold if the recovery process is carried out over samples that contain data modulations. For instance, with BPSK, the received MF samples are either the pair of $\{I_k = \cos(\theta_k + 0°), Q_k = \sin(\theta_k + 0°)\}$ or the pair of $\{I_k = \cos(\theta_k + 180°), Q_k = \sin(\theta_k + 180°)\}$.

The extraction of phase error can be performed as shown in Figure 4. By inspection of the x-y decomposition of the symbol energy ($real(Z_k)$ and $Imag(Z_k)$) that are rotated from their nominal position, one can easily conclude that the rotation error can be derived from the magnitude of Q.

Unfortunately, one has to know whether the phase error is that associated with a transmitted '0' or transmitted '1' before jamming the NCO with the correction signal. Fortunately, the magnitude of I again is used as a decision mechanism to resolve this uncertainty.

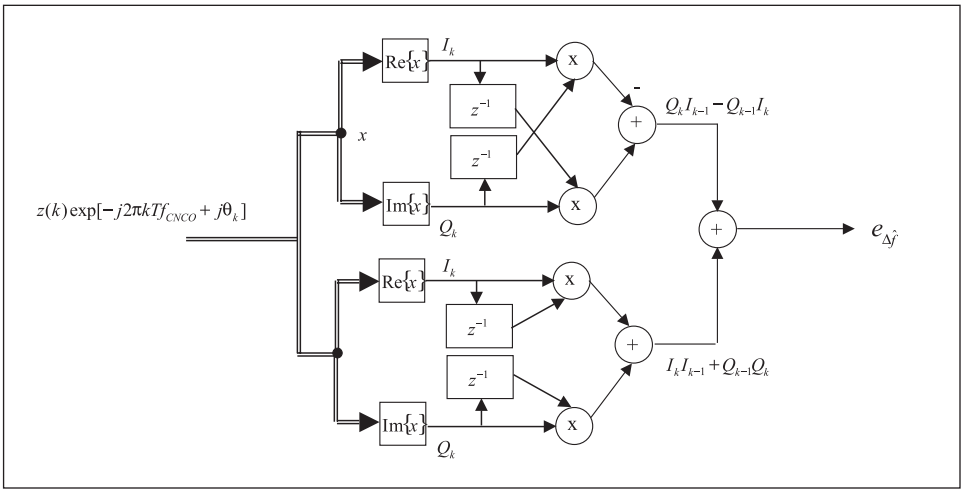

▲ **Figure 3. Frequency error detector for the CW signal.**

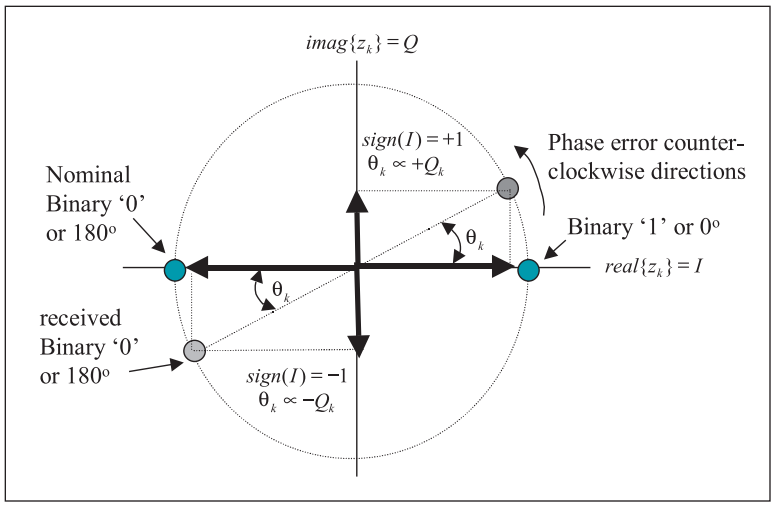

▲ **Figure 4. Detection and resolution of carrier phase error for modulated BPSK signals.**

As demonstrated in Figure 4, if the magnitude of I is positive ($sign(I)$ is positive), then the phase error is that associated with a binary '1.' Otherwise, the phase error is associated with a binary '0."

So for a BPSK, the phase error is given by $\theta_k = Q_k$ for the first pair and $\theta_k = -Q_k$ for the second pair. The negative sign of the error is coupled with the sign of the I channel. Therefore, the sign of the I channel can be used to generalize a formula for the carrier phase error associated with BPSK modulated signals. That is,

$$\theta_k = \begin{cases} +Q_k & I > 0 \\ -Q_k & I < 0 \end{cases} \tag{7}$$

or simply

$$\theta_k = Q_k sign(I_k) \tag{8}$$

m	$\frac{\pi}{4} + m\frac{\pi}{2}$	IQ	θ_k
0	$\frac{\pi}{4}$	11	$\frac{Q_k - I_k}{\sqrt{2}}$
1	$3\frac{\pi}{4}$	01	$-\frac{Q_k + I_k}{\sqrt{2}}$
2	$5\frac{\pi}{4}$	00	$-\frac{Q_k - I_k}{\sqrt{2}}$
3	$7\frac{\pi}{4}$	10	$\frac{Q_k + I_k}{\sqrt{2}}$

▲ **Table 1. Phase error signal for QPSK modulated signals.**

The error signal in Equation (8) indicates that all of the signal energy should be in the I channel when the BPSK signal is perfectly synchronized, that is, after the sine of I channel distinguishes the polarity of the error signal.

For QPSK and OQPSK modulated signals, the phase error detector must exhibit four-fold symmetry about the four possible phase angles of the MF samples. The in-phase and quadrature phase QPSK MF samples at the output of the quadrature demodulator with the unknown phase error θ_k is given by

$$I(k) = \cos\left(\theta_k + \frac{\pi}{4} + m\frac{\pi}{2}\right), \text{for } m = 0,1,2,3 \tag{9}$$

and

$$Q_k = \sin\left(\theta_k + \frac{\pi}{4} + m\frac{\pi}{2}\right), \text{for } m = 0,1,2,3 \tag{10}$$

Here the phase error signal can be obtained for each constellation point separately. Consider the case for m = 0, where the in-phase sample is given by

$$I_k = \frac{\sqrt{2}}{2}\left[\cos(\theta_k) - \sin(\theta_k)\right] \tag{11}$$

and the quadrature phase sample is given by

$$Q_k = \frac{\sqrt{2}}{2}\left[\cos(\theta_k) - \sin(\theta_k)\right] \tag{12}$$

When θ_k is small (i.e., the loop is in tracking mode), the carrier phase error signal can be generated by obtaining the difference of Equations (11) and (12):

$$\theta_k = \frac{Q_k - I_k}{\sqrt{2}} \tag{13}$$

Similarly, the error signal can be extended for the rest of the QPSK symbols. Table 1 lists the error signal for m = 1, 2 and 3.

The error detector can be generalized by

$$\theta_k = Q_k sign(I_k) - I_k sign(Q_k) \tag{14}$$

as shown in Table 1.

If the incoming carrier is modulated by a pair of alternating sequence of QPSK symbols as in Figure 1 (where the symbols are alternating pairs with 180 degrees of

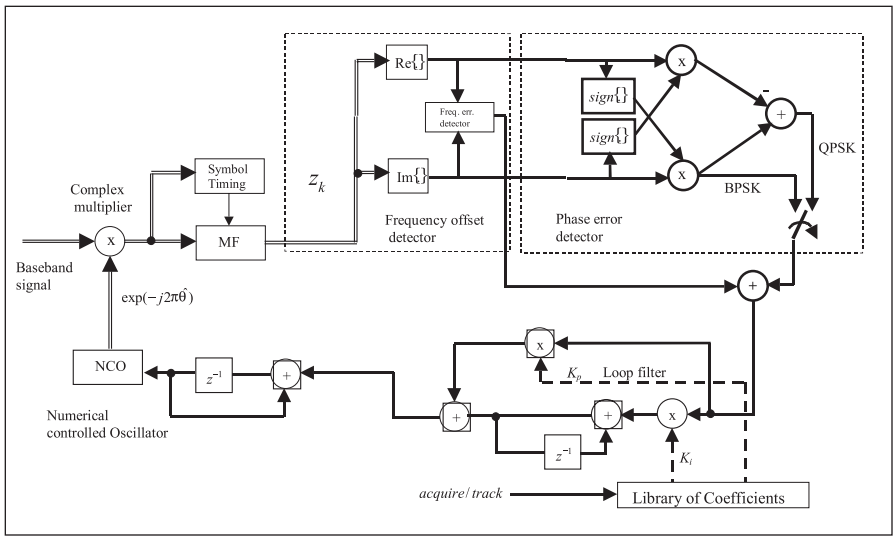

▲ **Figure 5. Bursts carrier offset acquisition and tracking loop for QPSK/BPSK.**

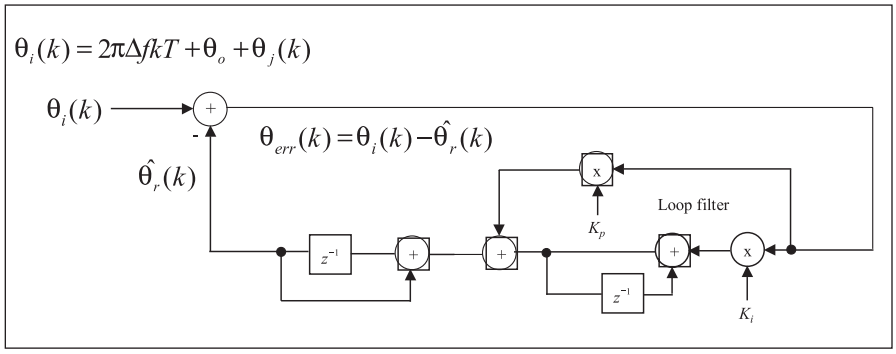

▲ **Figure 6. Linear model for the carrier recovery system shown in Figure 4.**

phase difference, for instance $\{I_k = 11, Q_k = 00\}$), the carrier phase error is given by

$$\theta_k = sign(I_k)\frac{Q_k - I_k}{\sqrt{2}} \tag{15}$$

Similarly, for the preamble pair of $\{I_k = 01, Q_k = 01\}$, the carrier phase error is given by

$$\theta_k = sign(I_k)\frac{Q_k + I_k}{\sqrt{2}} \tag{16}$$

Digital QPSK/BPSK carrier acquisition and tracking loop

Based on the error signals derived above, one way to implement an all-digital carrier recovery system for QPSK and BPSK modems is shown in Figure 4. Here digitized IF samples are translated down to baseband or passband by a complex numerically controlled oscillator (CNCO) and a complex multiplier (widely known as NCOM). The samples are then passed to the MF, which is implemented using an interpolator filter in conjunction with a decimator [2]. The interpolator filter is a FIR filter whose coefficients are controlled by an off-line timing symbol recovery algorithm as described in [2].

The in-phase (I) and quadrature (Q) MF outputs are then input to a carrier error signal detector. The frequency error detector and phase-offset detector are used in conjunction with a common loop filter to complete the feedback control system. The loop filter can be programmed during initial power up of the receiver to establish carrier frequency offset recovery.

Once the offset is removed, the loop filter is loaded again with another set of coefficients to perform carrier phase tracking.

Acquisition time and loop filter design

The bandwidth of the loop filter (in Figure 5) and the symbol rate (loop iteration rate) establish the performance of the carrier recovery feedback system in terms of acquisition time and offset frequency capture range. A larger loop bandwidth has shorter acquisition time, but provides a noisier control signal, which results in higher phase error variance. Usually, the loop bandwidth is set between 5 to 10 percent of the symbol rate [8]. This has been shown to offer a maximum capture range of frequencies up to twice the loop bandwidth [2]. Thus, for the 10 kbps system, the maximum frequency "pull in" range is 1000 hertz with

$$B_L = 0.05\left(\frac{1}{T}\right)$$

Figure 6 shows one linearized model of the system shown in Figure 5.

The loop filter is implemented by a direct gain K_p (proportional gain) path and an integrated path K_i (integrator gain) to filter frequency discriminator error signals. The filter is a Type-II loop filter whose steady state error converges to zero for both phase and frequency offsets [8] and can track a changing frequency rate proportional to the loop bandwidth. As shown in Figure 6, the input phase error samples are given by

$$\theta_i(k) = 2\pi\Delta fkT + \theta_o + \theta_n(k) \tag{17}$$

where Δf is the initial frequency offset, θ_o is the initial

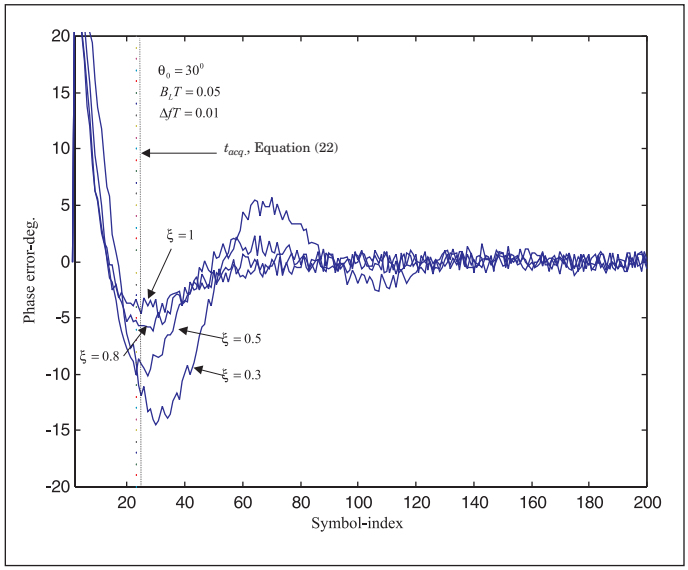

▲ **Figure 7. Impact of damping factor ξ on carrier tracking.**

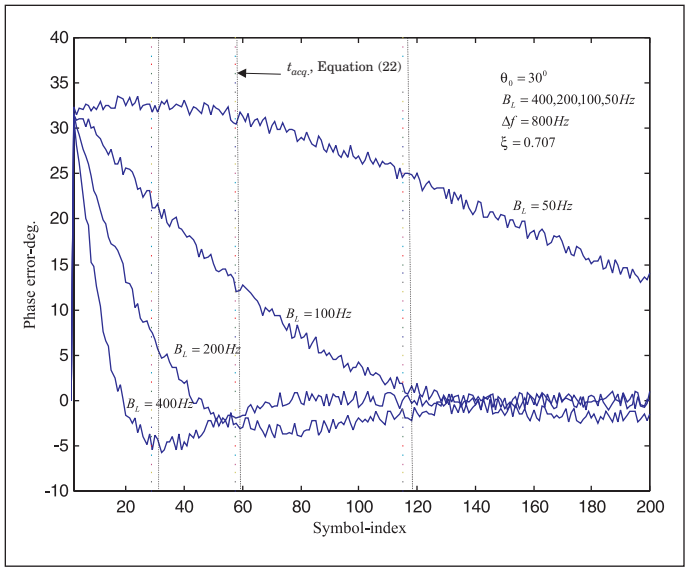

▲ **Figure 8. Impact of loop bandwidth (B_L) on carrier acquisition.**

carrier phase and $\theta_n(k)$ is an AWGN. The system function is

$$\frac{\hat{\theta}_r(z)}{\theta_i(z)} = \frac{K_p + K_i\left(z - \dfrac{K_i}{K_p + K_i}\right)}{z^2 - 2\left(1 - \dfrac{K_p + K_i}{2}\right)z + \left(1 - K_p\right)} \tag{18}$$

The loop filter parameters K_p and K_i are designed to minimize the phase and offset errors while yielding minimum acquisition time. Both parameters are given by

$$K_p = 2\xi\left(\frac{2B_L T}{\xi + \dfrac{1}{4\xi}}\right) \tag{19}$$

$$K_i = \left(\frac{2B_L T}{\xi + \dfrac{1}{4\xi}}\right)^2 \tag{20}$$

where B_L is the noise loop bandwidth, ξ is the second order damping factor and T is the symbol rate (i.e., loop iteration rate) [8]. Given a set of desired receiver parameters, Equations (17) through (20) can be used by computer-aided tools to optimize the carrier recovery loop for optimal timing acquisition and phase error variance. The error variance of the recovered carrier phase is directly proportional to the loop bandwidth B_L and is given by

$$\sigma_\theta^2 = \frac{B_L T}{E_s / N_o} \tag{21}$$

The required loop bandwidth in Equation (21) is directly obtained using a desired minimum BER degradation according to Equations (7-21) in [2]. For instance, assume a QPSK system with BER of 10^{-5} at E_s/N_o = 13 dB; for maximum BER deterioration of less than 1 dB, the required loop bandwidth B_L is 2000 hertz for the 10 kbps system (20 percent of the data rate). This value is used in conjunction with acquisition time requirements into the linear model to optimize the loop timing and stability behaviors.

Performance simulation results

Having established the loop parameters using Equations (19), (20) and (21), the effect of ξ and $B_L T$ on the dynamic response of the loop can be examined.

Let θ_o = 30°, $\Delta f T$ = 0.01 and $B_L T$ = 0.05. Figure 7 presents the response of the phase detector output $\theta_{err}(k)$ versus sample index (time) for various damping factors ξ. Notice that the loop is eventually able to drive the phase error $\theta_{err}(k)$ to zero.

As expected, the transient response of $\theta_{err}(k)$ becomes more oscillatory as ξ gets smaller than 1. Traditionally, for Type-II loops, a damping factor of ξ = 0.707 is a considered as an optimal choice for carrier recovery [2, 8].

It is commonly suggested that the loop filter damping ratio ξ has little impact on acquisition time. Based on this, the acquisition time for a second-order loop can be approximated by

$$t_{acq.} = \frac{1.2}{B_L T} \quad \text{[symbols]} \tag{22}$$

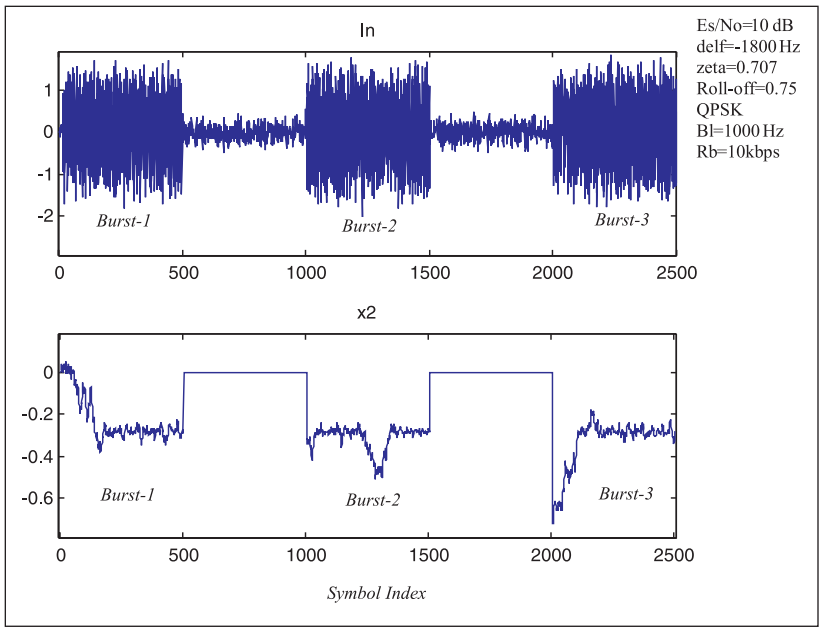

▲ **Figure 9. Carrier acquisition and tracking of three consecutive bursts at –1.8 kHz offset.**

The impact of the loop bandwidth on the transient response for the second-order carrier recovery loop, as well as the analytical values of t_{acq} were obtained using Equation (22) and are presented in Figure 8 [8]. Figure 8 illustrates a plot of the phase error signal $\theta_{err}(k)$ versus sample index (time) for various values of $B_L(B_L$ = 400, 200, 100 and 50) for Δf = 800 hertz and ξ of 0.707.

Because B_L does not change the oscillatory nature of the system, it can be concluded that B_L only affects the tracking-speed of the loop. Further, there is acceptable agreement between t_{acq} using Equation (22) and that obtained using simulations.

For larger B_L, the tracking speed is increased, but the loop's noise-suppression ability is reduced, thus increasing the phase error variance and ultimately degrading the receiver BER performance. For small B_L, the noise is reduced, but the tracking speed is degraded, as shown by Equation (22). This tradeoff becomes a limiting factor when this scheme is used for burst type systems.

Burst satellite QPSK carrier acquisition and tracking

Figure 9 shows an input of three consecutive bursts of 500 symbols of shaped QPSK and the error detector output after acquisition and tracking for the loop illustrated in Figure 4. The MF symbols had an intentional frequency offset of Δf = –1800 hertz. The bursts were fed into the proposed carrier recovery scheme of Figure 4, operating with B_L = 1000 hertz, V = 0.707 and E_s/N_o = 10 dB. Once the loop settled, the NCO was automatically set by the loop to the frequency

$$f = \frac{1}{T_{pb}} + \Delta f = 8200 \text{ hertz}$$

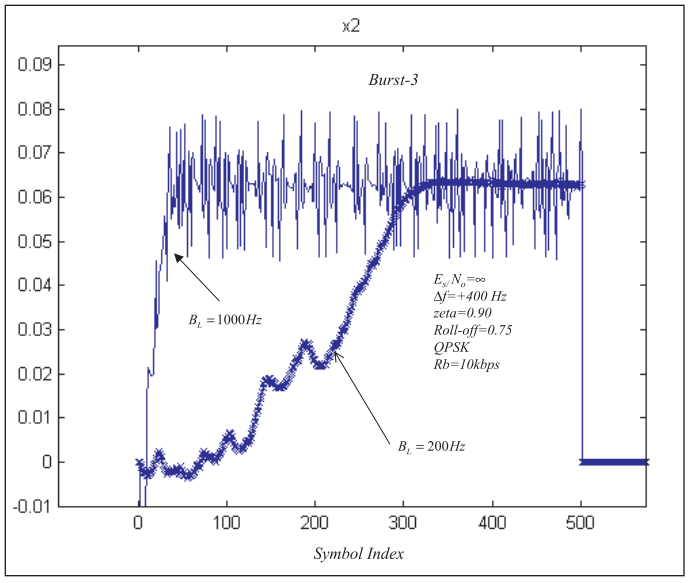

▲ **Figure 10. Comparison of frequency acquisition with two different loop bandwidths.**

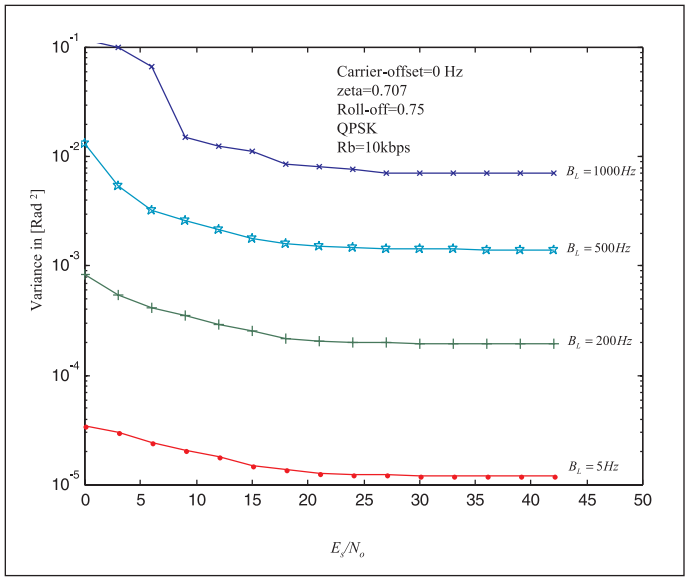

▲ **Figure 11. Variance of phase tracking error for several loop bandwidths.**

where T_{pb} is the nominal passband frequency.

Though the loop acquires quickly, the phase of the derived error is perturbed by the AWGN and never decays to zero. Note that the variance of this random phase error can be reduced by decreasing the loop bandwidth, but will result in a narrower capture range.

Figure 10 shows a comparison between acquisition performance of the proposed system for two different loop bandwidths in acquiring and tracking an offset of $\Delta f = +400$ hertz. If $B_L = 1000$ hertz, the loop acquires in less than 50 symbols, which sounds excellent for a 500 symbol burst. However, the loop error signal is perturbed by AWGN, causing phase modulations (phase noise) in the CNCO signal and resulting in an unacceptable random symbol rotation.

By lowering the loop bandwidth to $B_L = 200$ hertz, the final phase random walk is heavily damped (see Figure 9). However, it took an unacceptable 350 symbols for the receiver to acquire and track the carrier frequency offset of 400 hertz. The final phase variance was monitored using Monte-Carlo analysis with 20,000 transmitted QPSK symbols (40 bursts).

The same experiment was repeated for 100 consecutive bursts using different loop bandwidths and then the final tracking error variance was calculated. Figure 11 shows plots of the tracking phase error variance against E_s/N_o for loop bandwidths of $B_L = 1000$, 500, 200 and 50 hertz. Clearly, in all of these cases, the variance approaches an irreducible value for E_s/N_o larger than 16 dB. The final phase variance is reduced from $\sigma_\theta = 5.73$ degrees at $B_L = 1000$ hertz to less than $\sigma_\theta = 0.005$ degrees at $B_L = 5$ hertz.

In general, the phase error variance obtained using the Monte-Carlo experimental simulations in Figure 11 is bounded by the analytical variance given by

$$\sigma_\theta^2 = \frac{B_L T}{E_s / N_o}\left[\text{rad}^2\right] \tag{23}$$

Using Equation (23), with $E_s/N_o = 10$ dB and a loop bandwidth of 5 hertz, yields a theoretical value of 1×10^{-5} [rad^2], which highly matches that obtained using the simulated scheme in Figure 5, as shown in Figure 11.

Conclusion

This article has illustrated technical details, performance and experimental simulations of an all-digital carrier acquisition and recovery algorithm suited for modern software-based wireless radio. The algo-

rithm is able to acquire and track the carrier of a short burst TDMA frame reliably and rapidly. The carrier frequency and phase error detectors used were extended to operate not only over a CW preamble, but also during the presence of data modulations. From a hardware-complexity point of view, this algorithm is efficient to implement, since most of its functions are used in most digital down converters (complex multiplier and NCO) used to translate the received channel from a sampled IF into baseband. ■

References

1. MIL-STD-188-181, Department of Defense Standards, "Interoperability Standard for Single-Access 5kHz and 25kHz UHF Satellite Communications Channels," March 20, 1999, U.S. DoD.

2. Heinrich Meyr and Gerd Ascheid, *Synchronization in Digital Communications*, Vol. 1, New York: John Wiley & Sons, 1989.

3. M. Nezami and R. Sudhakar, "M-QAM Digital Symbol Timing Synchronization in Flat Rayleigh Fading Channels," *PRMIC*, Osaka, Japan, November 1999.

4. Tri T. Ha, *Digital Satellite Communications*, New York: McGraw-Hill, 1990.

5. Edward W. Chandler, "A Frequency Tracking Technique for Multiple Access Satellite Communication Networks," *TCC*, 1990.

6. M.K. Nezami and R. Sudhakar, "DFT-Based Frequency Acquisition Algorithm for Large Carrier Offsets in Mobile Satellite Receivers," *IEE Electronics Letters*, March 2001.

7. M.K. Nezami, "Overview of DSP-Based Feed Forward Carrier Offset Recovery Algorithms used in Satellite and Cellular Receivers," *ICSPAT*, Dallas, TX, October 16-19, 2000.

8. F.M. Gardner, *Phase Techniques*, 2nd edition, New York: John Wiley & Sons, 1979.

9. Harris Semiconductor, "The NCO as a Stable, Accurate Synthesizer," Application Note, 1993, www.intersil.com.

Author information

Mohamed Nezami received both a bachelor of science and master of science degrees in electrical engineering from the University of Colorado, Denver, in December 1988 and 1990, respectively. He received a Ph.D. in electrical engineering from Florida Atlantic University, Boca Raton, in March 2001. He has been involved in wireless radio design for 10 years. Currently, he is working for Raytheon Company in St. Petersburg, FL. His research interests include digital receiver algorithms, wireless systems and RF and microwave circuits. He can be reached at E-mail: mkna@stp.us.ray.com; or Tel: 727-725-0486.